CEA/DAPNIA/SEA-97-17

Design of a final focus system for CLIC in the multi-bunch regime

Olivier NAPOLY

CEA, DSM/DAPNIA/SEA
CEA/Saclay, F-91191 Gif-sur-Yvette Cedex, France

December 10, 1997

Abstract

We present a design for the CLIC final focus system which authorizes the stable multi-bunch operation with a 5 mrad crossing-angle. The loss of luminosity is limited to less than 20% in such a way that crab-crossing cavities may not be required. The main feature of the design is that the vertically focusing final quadrupole is split into a 48 mm large bore superconducting quadrupole and a 13.7 mm bore normal conducting one. In that way, the off-axis outgoing beam is deflected by the first quadrupole into the field-free region of the second one.

1 Introduction

The preceding final focus systems for CLIC had been designed for the single bunch operation at zero crossing-angle. With the current CLIC parameters, partially recalled in Table 1, 60 bunches separated by 20 cm (0.67 ns) form a bunch train repeated at 511 Hz rate. To avoid unwanted collisions at multiples of 10 cm distances away on both sides from the IP, it is necessary to include a non-zero crossing-angle. This crossing angle must be large enough to stabilize the bunch train from the multi-bunch kink instability generated by the parasitic crossings. If the crossing angle is larger than the "diagonal" angle of the beam $\alpha_\Delta = \sigma_x/\sigma_z$, the loss of luminosity is significant. It can be completely recovered with the crab-crossing scheme using transversely deflecting RF cavities to rotate the bunches around their vertical axis. This scheme, adopted in the NLC [1] and JLC [2] designs, can certainly be adapted to the CLIC parameters as well.

In this study, we would like to investigate an alternative scheme where crab-crossing is not required but left as an optional improvement. This is possible because the diagonal angle α_Δ is 4.12 mrad for the CLIC parameters, that is small enough to consider a 5 mrad crossing angle with a loss of luminosity limited to 20%, and even less with some dispersion induced crab-crossing [3] much simpler to implement. We therefore attempt to design a final focus system less complex than the NLC design, that is with fewer and simpler quadrupoles and no crab-crossing cavities. In this design the beam extraction angle, starting from the initial crossing-angle of 5 mrad is increased to 9 mrad by the deflection provided by the first quadrupole, with a large aperture, to the off-axis outgoing beam trajectory. This trajectory then crosses the field-free region of the other smaller aperture quadrupoles of the last doublet.

Beam sizes	σ_x^*, σ_y^*	[nm]	206 , 5.4
Emittances	$\gamma\epsilon_x^*, \gamma\epsilon_y^*$	[μm]	1.88 , 0.10
Bunch length	σ_z	[μm]	50
Bunch population	N_e	[10^{10}]	0.4
Number of bunch per train	n_b		60
Bunch spacing	Δt_b	[ns]	0.67
Divergences	θ_x^*, θ_y^*	[μrad]	19 , 38
Beta	β_x^*, β_y^*	[mm]	11 , 0.143

Table 1: CLIC beam parameters at the IP for $\sqrt{s} = 500$ GeV

2 Crossing-Angle and Multi-bunch Kink Instability

In this section we discuss the choice of the crossing angle and its implication on the luminosity.

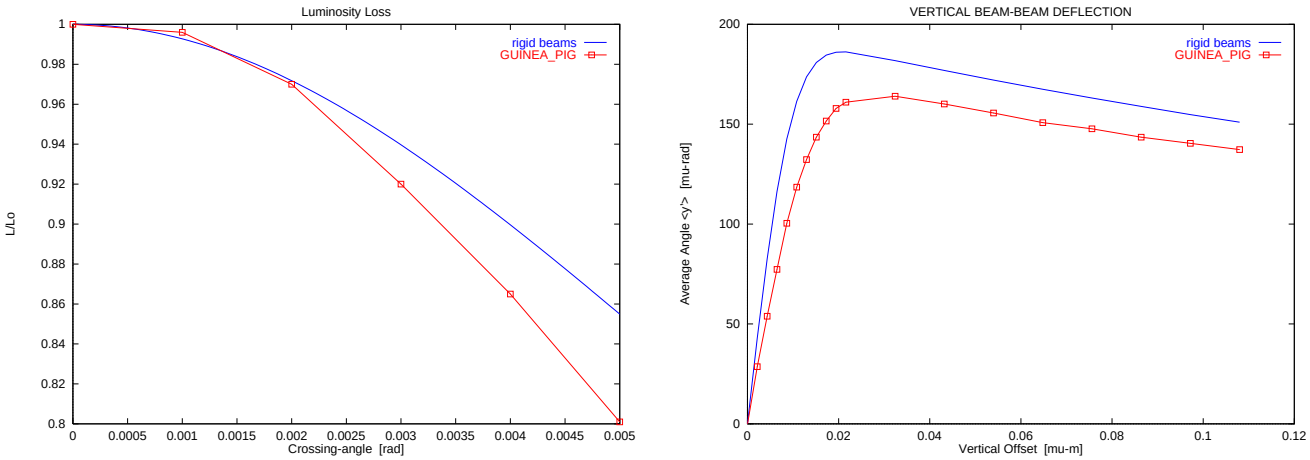

(a) (b)

Figure 1: Luminosity loss vs. crossing angle (a) and beam deflection vs. offset (b).

2.1 Single bunch luminosity

For rigid beams, the luminosity as a function of the crossing angle α is given by the following expression

$$\mathcal{L} = \mathcal{L}_0 \cdot \frac{1}{\sqrt{1 + (\tan(\alpha/2)/\alpha_\Delta)^2}} \tag{1}$$

where the diagonal angle is $\alpha_\Delta = \sigma_x/\sigma_z = 4.12$ mrad for CLIC. It is therefore expected that the luminosity loss is small for crossing angles smaller than α_Δ. The actual luminosity loss including the beam-beam effect simulated with GUINEA_PIG [4] is shown in Fig.1(a) in comparison with the rigid beam expression. The expected loss is 20% for a 5 mrad crossing-angle. However, because of the energy correlation along the bunch, the luminosity at finite crossing-angle can be better optimized for the non-zero horizontal dispersion that achieves a partial crab-rotation [3] of the bunches. The expected gain in luminosity has not been calculated.

2.2 Multi-bunch luminosity

To estimate the loss of luminosity from the multi-bunch instability induced by the parasitic crossings, one must first calculate the coherent beam-beam kick at the IP, which is the main source of the instability, as a function of the beam offset. This is done in Fig.1(b) where the result of a beam-beam deflection scan simulation with GUINEA_PIG [4] is compared to the rigid beam expression. The focal distance of the coherent beam-beam kick derived from the slope of the deflection curves at the origin is $f_{coh} = 74\ \mu m$ for the simulation and $f_{coh} = 50\ \mu m$ for rigid beams.

The first value is used to calculate the loss of luminosity averaged over the bunch train as a function of the incoming bunch-to-bunch vertical jitter. The results are shown in Fig.2 for three different values of the crossing-angle. For simplicity, in this calculation

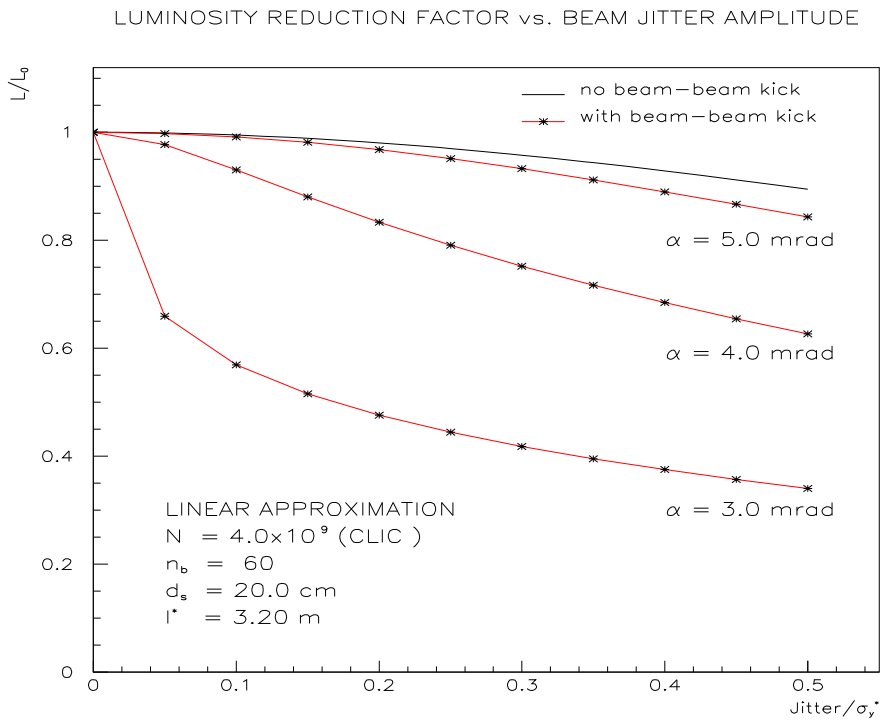

Figure 2: Multi bunch luminosity loss from bunch to bunch vertical jitter.

the 11.8 m long colliding bunch trains have been assumed to travel along a straight orbit around the IP and to be separated in two different beam pipes at $\pm 3.2\ m$ from the IP. As shown in Fig.3, in the proposed doublet design the first 3.2 m space actually includes a defocusing quadrupole from 1.5 to 2.7 m which provides an additional horizontal separation of the bunch trains. One can therefore expect the luminosity to be slightly larger than calculated. Moreover, although perfectly adequate to predict the onset of the instability, the linear approximation used for the beam-beam kicks overestimates this effect.

Fig.2 reveals an instable bunch train collision for 3 and 4 mrad, and a rather stable regime at 5 mrad. For instance, at this value the multi-bunch beam-beam effect only reduces the luminosity by 5% in addition to the expected 10% reduction for a jitter of half-σ_y.

3 Final Doublet and Interaction Region Design

The layout of the interaction region with a 5 mrad crossing incoming orbits is shown in Fig.3. Its main characteristics are summarized in Table 2. Each final doublet includes a focusing quadrupole QF and a split defocusing quadrupole (QD1,QD2). Splitting the defocusing quadrupole is necessary for the spent beam extraction as discussed in Sect.5. QD1 is a large aperture superconducting quadrupole : it is identical to the final doublet

Quadrupoles	Length [m]	Aperture diameter [mm]	Gradient [T/m]
QD1	1.2	48	250
QD2	1.378	13.7	219
QF	1.330	13.7	219
last drift	1.5		
between quads	0.50		

Table 2: Doublet parameters

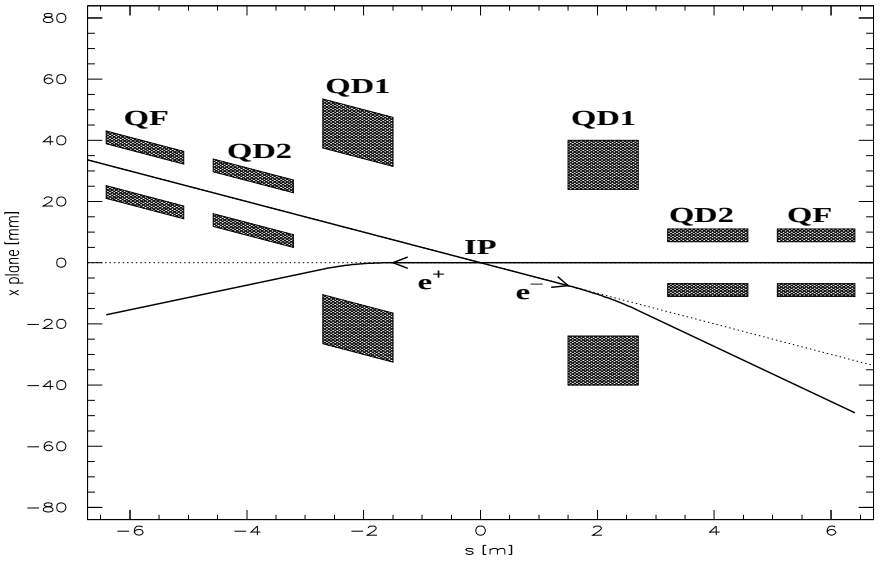

Figure 3: Magnet layout with a 5 mrad crossing-angle. The e^+ and e^- orbits (solid lines) correspond to the nominal energy of 250 GeV.

quadrupole designed for TESLA [5] from the LHC two-in-one lattice quadrupoles [6]. The quadrupoles QD2 and QF are normal conducting : they have the same aperture and cross-section as the JLC final doublet quadrupoles [2] and we have assumed a pole-tip field of 1.5 T.

Taking an outer radius of 150 mm for the QD1 cryostat, like for TESLA, and a cylindrical mask thickness of 50 mm around it, the dead cone in the forward region of the detector would be limited to an angle of 133 mrad, smaller than the JLC design. Furthermore, the 0.5 m distance between QD1 and the warm magnet QD2 is enough for the endcap of the cryostat. If the quadrupoles QD2 and QF, because of their iron yoke, need to be shielded from the detector solenoid field, a superconducting compensating solenoid could be included in the same cryostat.

4 Synchrotron Radiation from the Final Doublet

While the incoming beam stayclear conditions are $30\sigma_x$ and $74\sigma_y$, the clearing of the synchrotron radiation from the last doublet quadrupoles requires about $10\sigma_x$ and $20\sigma_y$ transverse collimation of the beams, as shown in Figs.(4,5). This is rather tight vertically when compared to the $40\sigma_y$ required for the JLC design with a 2 times smaller emittance. The profile of the synchrotron radiation from the upstream doublet for $20\sigma_x$ and $40\sigma_y$ collimation requirements at that phase is shown, by Fig.6, not to be a problem.

As shown in Fig.7, the Oide effect induced by the synchrotron radiation in the last doublet has a negligible impact on the spot sizes at the IP for the design emittances.

5 Spent Beam and Beamstrahlung Photon Extraction

The main characteristics of the spent beams and beamstrahlung photon beam are given in Table 3. Their angular and energy distributions are also represented in Figs.(8,10,11). Notice the asymmetry in the horizontal angular distribution of the photons due to the finite crossing-angle. These distributions are calculated from a GUINEA_PIG [4] beam-beam simulation using 40 000 macro-particles.

Spent Beams			
Emittances	ϵ_x, ϵ_y	[pm]	13 , 0.38
Divergences	θ_x, θ_y	[μrad]	106 , 99
Beta	β_x, β_y	[mm]	4.5 , 0.073
Beamstrahlung Photons			
Average angle	$\langle x'_\gamma \rangle$, $\langle y'_\gamma \rangle$	[μrad]	13 , 0
Divergences	$\theta_{\gamma,x}, \theta_{\gamma,y}$	[μrad]	66 , 78

Table 3: Spent beam and beamstrahlung photon beam parameters

With their very small angular spread, the extraction of the beamstrahlung photon beams is not a problem. On the contrary, extracting the low energy particles of the spent beams puts a constraint on the length of the first quadrupole QD1. If too low in energy or at a too large angle at the IP, these particles hit the exit face of the quadrupole. Given its 48 mm aperture diameter, the acceptance of this quadrupole in the energy E and horizontal angle x' phase-space of the particles originating from the IP, is shown in Fig.9 for three different quadrupole lengths. Using a 1.5 m long quadrupole would simplify the doublet design by allowing to remove the second defocusing quadrupole QD2. Unfortunately, Fig.9 clearly shows that such a quadrupole would be hit by a large number of outgoing particles. Using the $2\times40\,000$ macro-particle sample of the simulation, one can roughly estimate that the 1.2 m QD1 quadrupole should be hit by a fraction of the spent beam smaller than

$5 \cdot 10^{-6}$ representing about 25 W of beam power. This is certainly too large to be sustained by the cryostat. A finer estimate of the power deposited at the edge of the cryostat should include more particles in the beam-beam simulation as well as taking the contribution from the bremmstrahlung particles into account. If this power is too large, a back up solution should be found with a 1 m QD1 quadrupole or with a larger bore quadrupole like the low-β LHC ones. These quadrupoles, with a larger outer diameter, would however increase the dead cone in the detector.

6 Optics of the Chromaticity Correction

The doublet design described above can be combined into a final telescope with 12×30 de-magnification. Including a chromatic correction section with 2 pairs of sextupoles, the final focus system shown in Fig.13 is 560 m long. Its bandwidth is plotted in Fig.14 : it is about 1% wide. If this is too small for the single bunch energy spread, more sextupoles can be added in order increase the bandwidth [7].

7 Conclusion

We have proposed a final focus system design for CLIC based on a small crossing angle of 5 mrad and a scheme where the beams are focused and extracted by an hybrid doublet. The main advantage of the system over a crab-crossing scheme with a larger crossing angle as chosen for the NLC design, lies in its simplicity : fewer and simpler quadrupoles, easier design of the vacum chamber around the IP, no crab-crossing cavities.

However the viability of the proposed design must be studied in more details. In particular, the following questions should be investigated:

1. Validate the choice of a 5 mrad crossing-angle by detailed simulations of the multi-bunch kink instability. For instance, the additional separation induced by the first defocusing SC quadrupole will reduce the sensitivity of the luminosity to the incoming jitter.

2. Introduce crab-crossing with dispersion at the IP. This will reduce the 20% expected loss of luminosity due to the crossing angle.

3. Characterize the spent beam energy spectrum, in particular the cross-over at low energy with the irreducible bremsstrahlung spectrum.

4. Check the dependance of the beam-beam effect on the shape of the longitudinal distribution.

5. Refine the beam loss estimate from the extracted beam.

6. Increase the FFS bandwidth by adding sextupoles in the CCS.

7. Study the transverse coupling effect induced by the detector solenoid and the non-zero crossing angle.

Acknowledgements

I thank Daniel Schulte for many discussions, and Ian Wilson for inviting me several times to do this study.

References

[1] "Zeroth-order Design Report for the Next Linear Collider", LLBNL-PUB-5424, SLAC Report 474, UCRL-ID 124161, 1996.

[2] "JLC Design Study Report", DRAFT April 30 (1997). I thank T. Tauchi for providing me with the chapter 14 of this report.

[3] R. Brinkmann, "Crab-crossing with dispersion ", unpublished

[4] D. Schulte, "Study of Electromagnetic and Hadronic Background in the Interaction Region of TESLA", Ph.D. thesis, University of Hamburg 1996, and DESY report TESLA 97-08, April 1997

[5] "Conceptual Design of a 500 GeV e^+e^- Linear Collider with Integrated X-ray Laser Facility", R. Brinkmann, G. Materlick, J. Rossbach and A. Wagner Editors, DESY 1997-049 and ECFA 1997-182 (1997).

[6] J.M. Rifflet et al., "Cryogenic and Mechanical Measurements of the first two LHC lattice Quadrupole Prototypes", EPAC94 Conf., London, Great Britain, 1994.

[7] R. Brinkmann, "Optimization of a Final Focus System for Large Momentum Bandwidth", DESY-M-90-14, 1990.

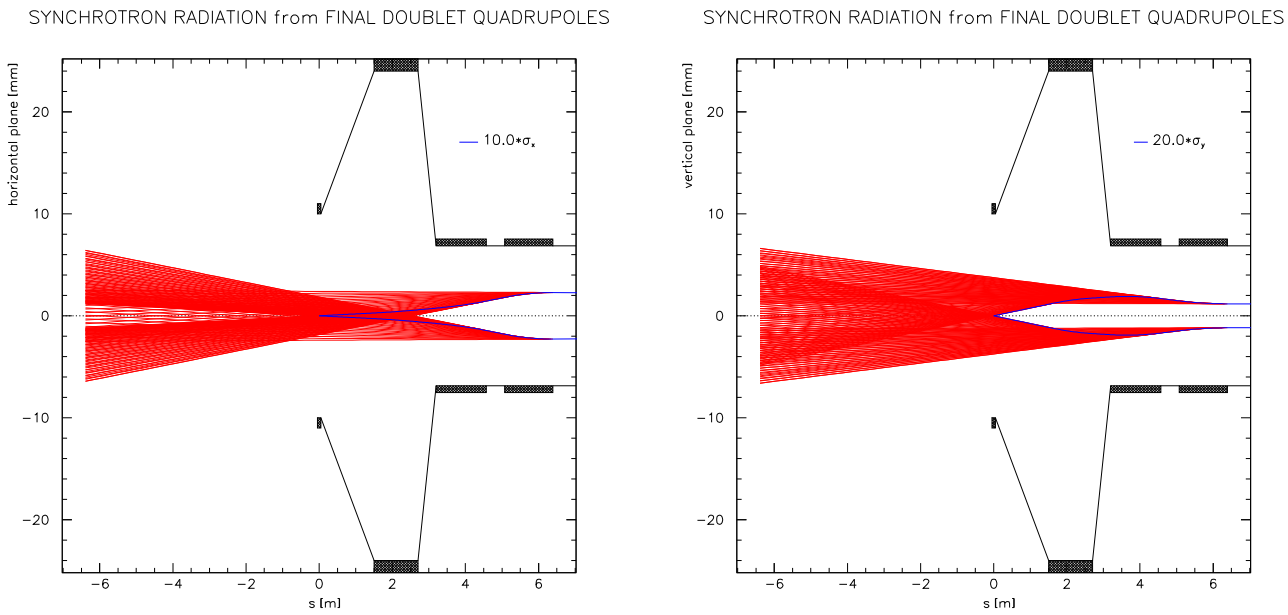

(a) (b)

Figure 4: Longitudinal profiles of the synchrotron radiation from the last doublet: (a) horizontal plane, (b) vertical plane.

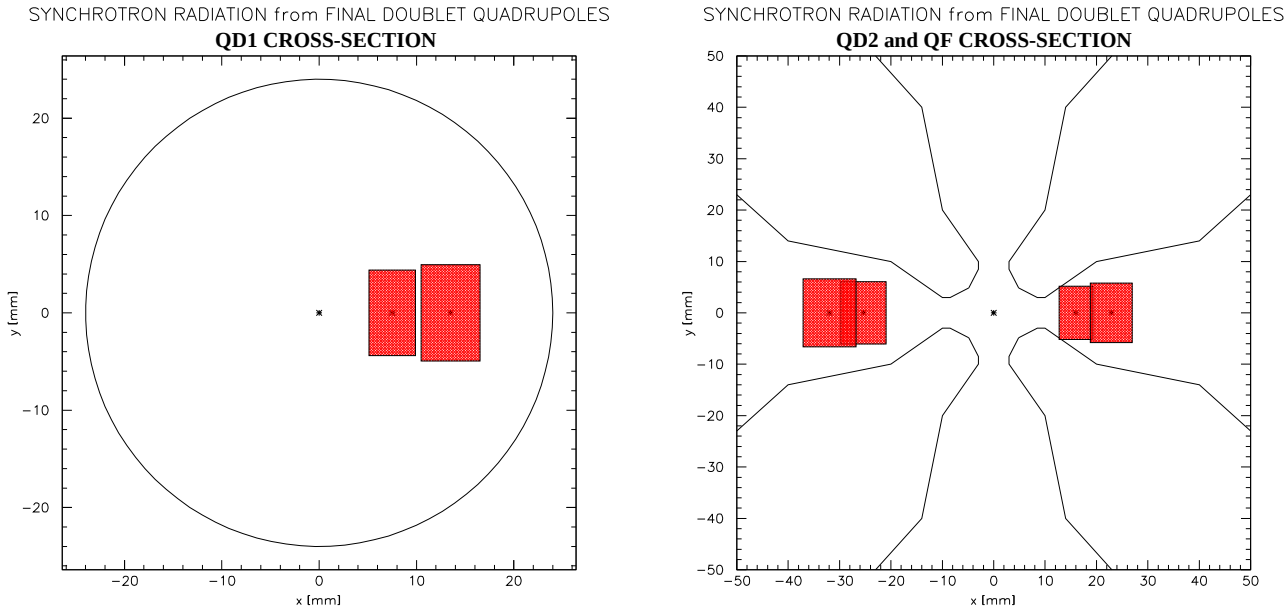

(a) (b)

Figure 5: Transverse profiles of the synchrotron radiation at the entrance (small rectangle) and exit (large rectangle) faces of : (a) QD1, (b) QD2 (right) and QF (left) in the extraction line.

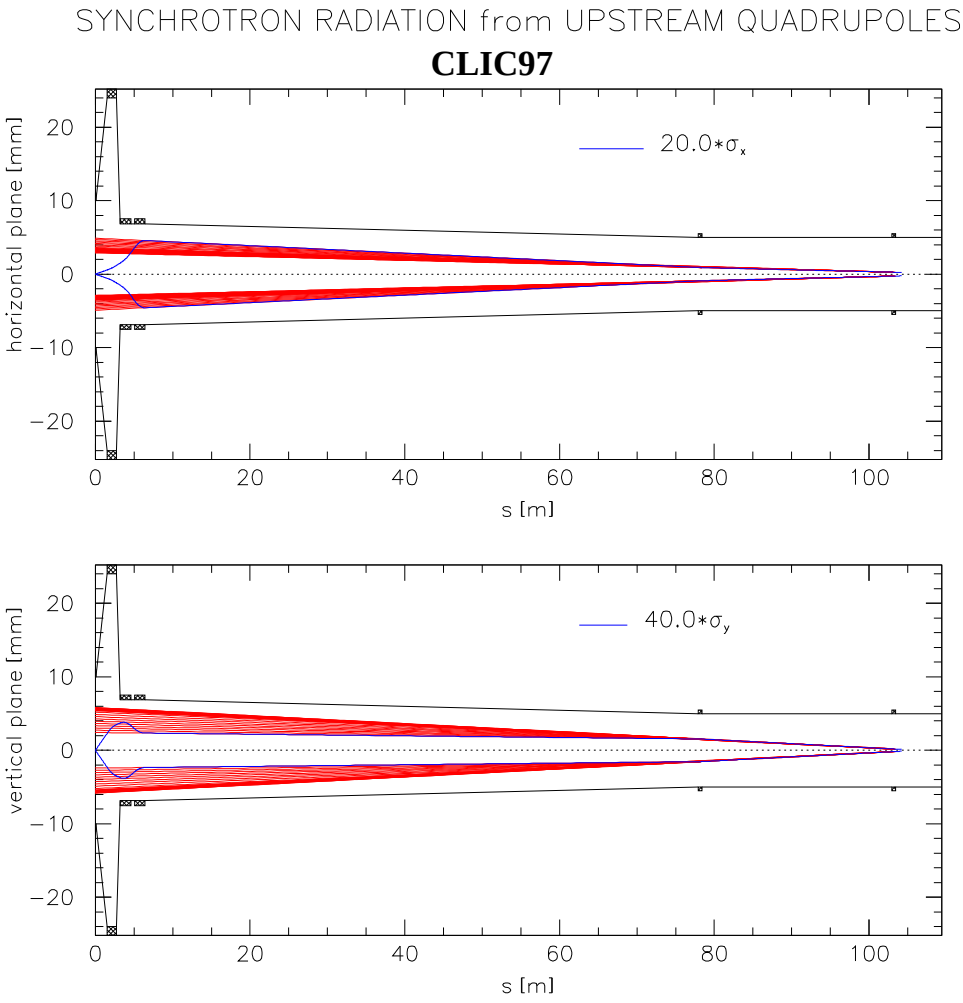

Figure 6: Longitudinal profiles of the synchrotron radiation from the last but one doublet.

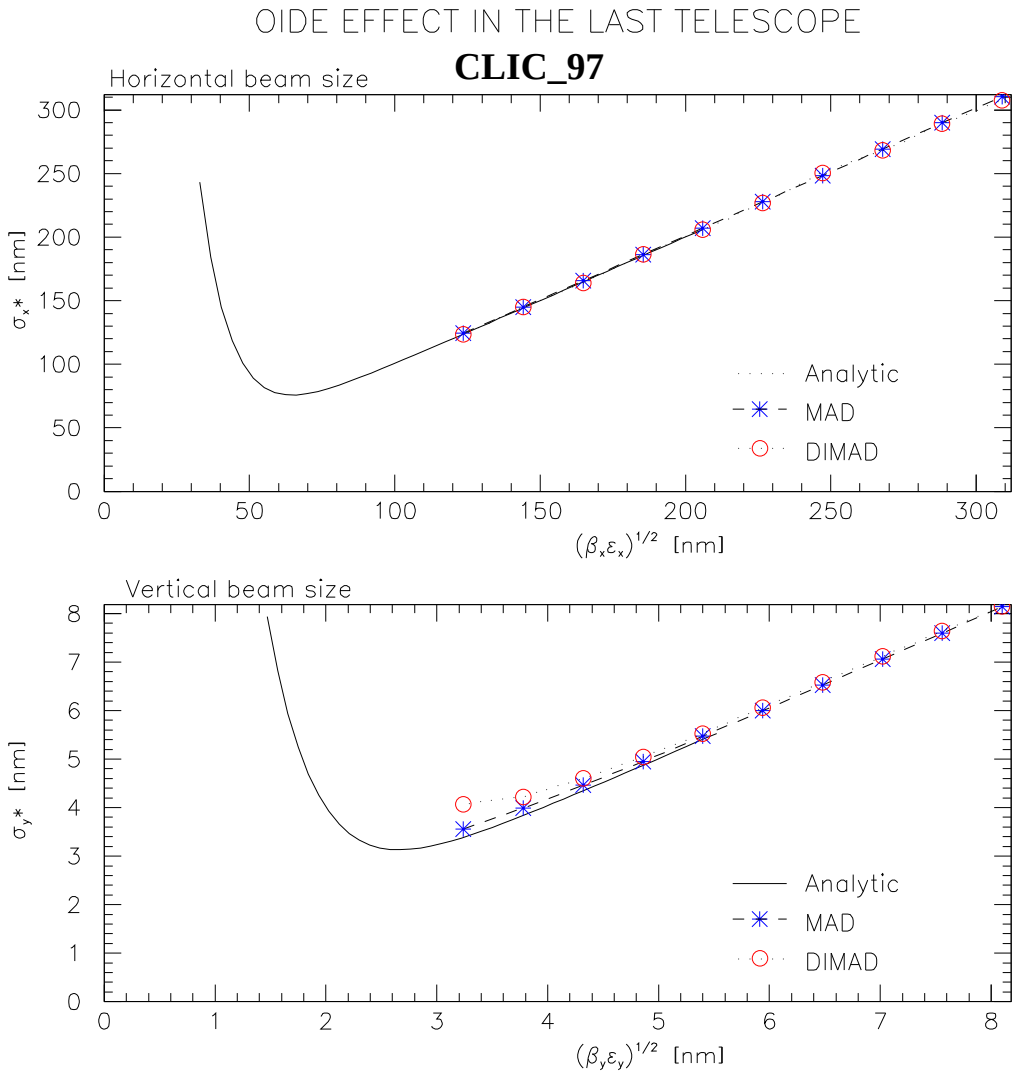

Figure 7: Oide effect in last doublet.

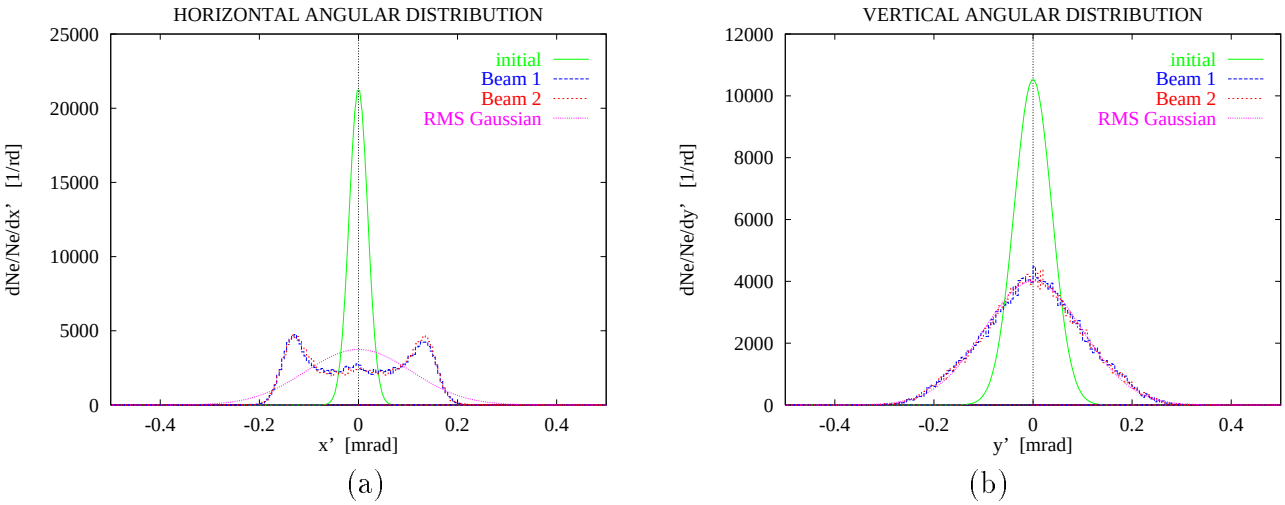

Figure 8: Spent beam angular distribution: (a) horizontal plane, (b) vertical plane.

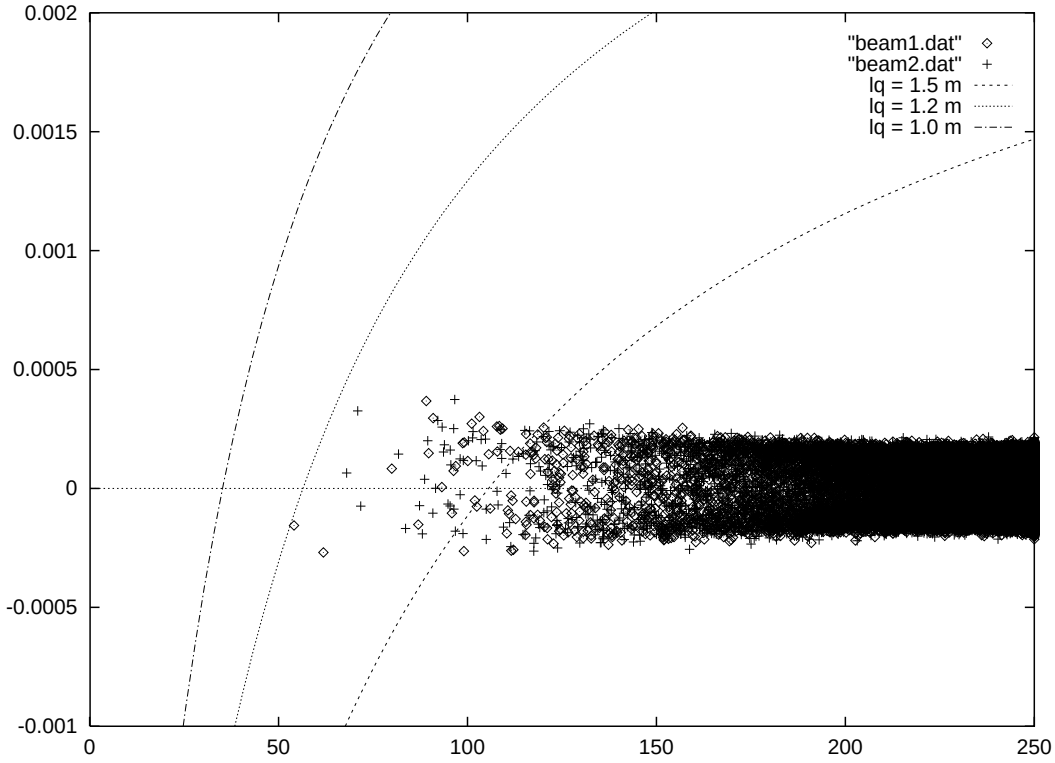

Figure 9: Acceptance of the large aperture quadrupole QD1 of 1 m, 1.2 m or 1.5 m length in the E [GeV]-x' [rad] plane. These limits are compared to the distribution of the $2 \times 40\,000$ spent beam particles as predicted by GUINEA_PIG.

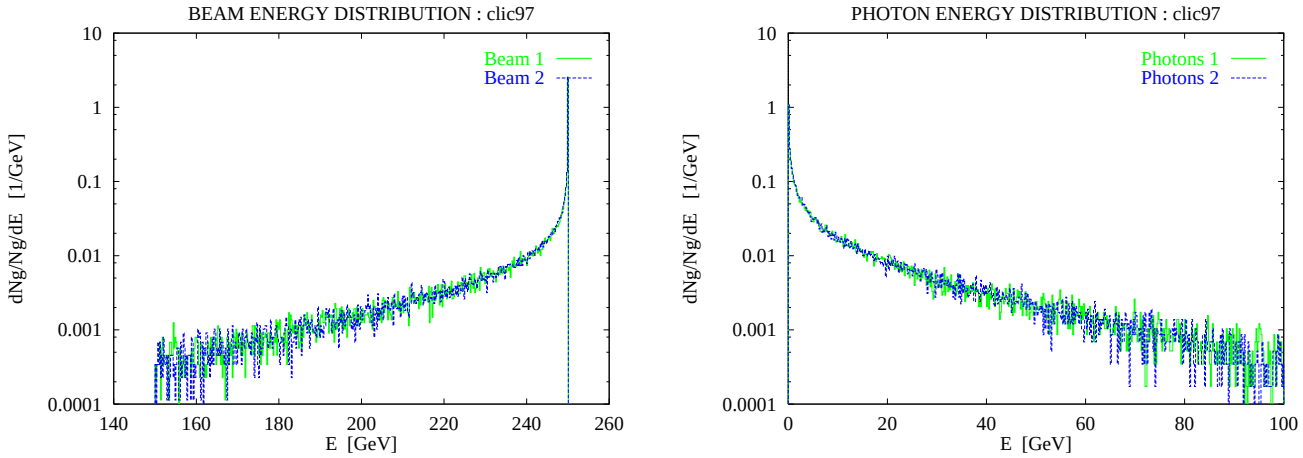

(a) (b)

Figure 10: Energy distribution: (a) spent beam, (b) beamstrahlung photon.

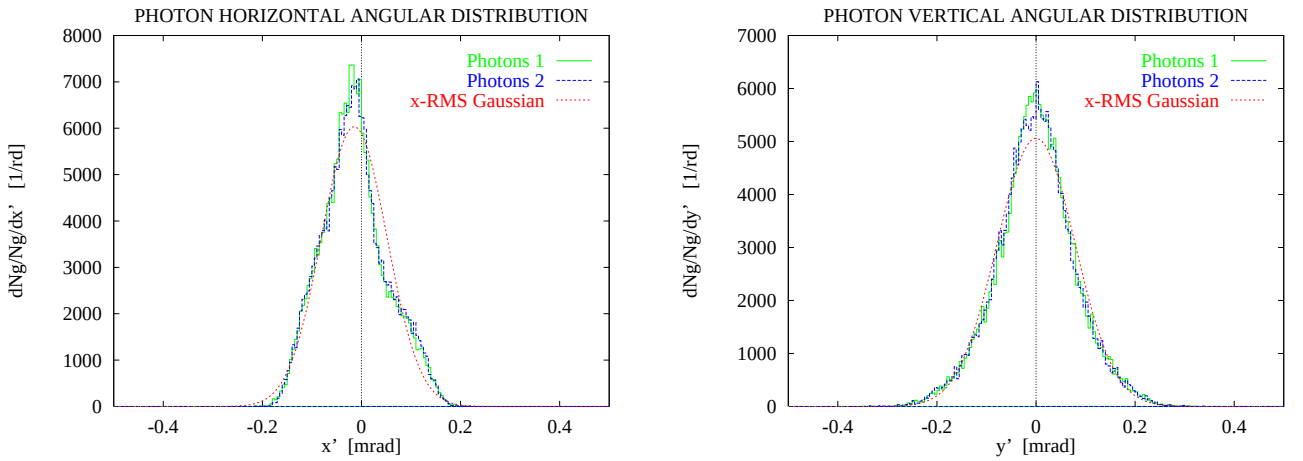

(a) (b)

Figure 11: Beamstrahlung photon angular distribution: (a) horizontal plane, (b) vertical plane.

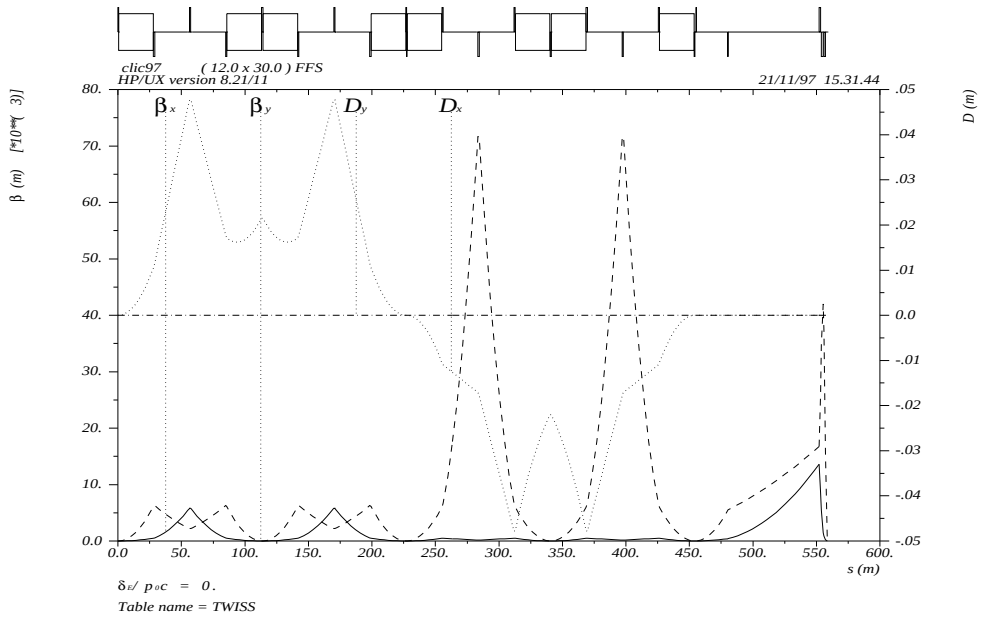

Figure 12: Optics of the chromatic correction section

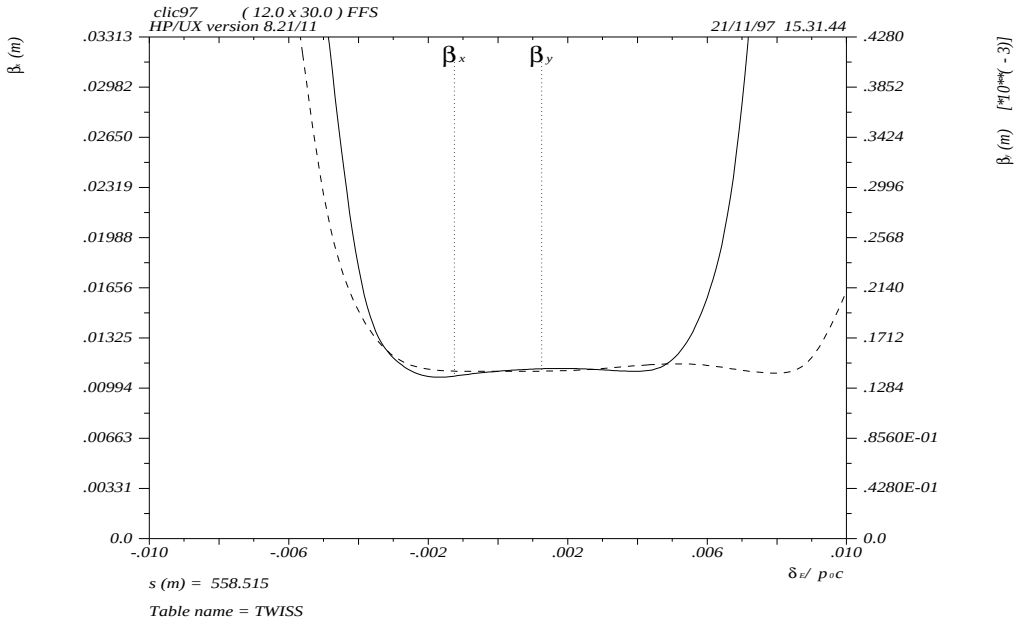

Figure 13: Bandwidth of the chromatic correction section